Annals of Botany **104**: 621–633, 2009
doi:10.1093/aob/mcp144, available online at www.aob.oxfordjournals.org

ANNALS OF BOTANY
Founded 1887

Developmental changes in spatial distribution of *in vivo* fluorescence and epidermal UV absorbance over *Quercus petraea* leaves

S. Meyer[1,*], J. Louis[1], N. Moise[2], T. Piolot[3], X. Baudin[3] and Z. G. Cerovic[1]

[1]*Laboratoire Ecologie Systématique et Evolution, CNRS, UMR 8079 (CNRS, UPS, AgroParisTech), Université Paris-Sud, Bât. 362, F-91405 Orsay, France,* [2]*Force-A, Université Paris-Sud, Bât. 503, F-91405 Orsay, France and* [3]*Plate-forme de recherche 'Imagerie des processus dynamiques en biologie cellulaire et biologie du développement', Institut Jacques Monod, UMR 7592 CNRS, INSERM, Université Paris Diderot-Paris7, Bât. Buffon, F-75013 Paris, France*

Received: 24 March 2009 Returned for revision: 23 April 2009 Accepted: 1 May 2009 Published electronically: 27 June 2009

• *Background and Aims* Epidermal phenolic compounds (mainly flavonoids) constitute a vital screen that protects the leaf from damage by natural ultraviolet (UV) radiation. The effectiveness of epidermal UV-screening depends on leaf anatomy, the content of UV-screening compounds and their spatial uniformity over the leaf area. To investigate *in vivo* the spatial pattern of the epidermal UV-screen during leaf development, a fluorescence imaging method was developed to map the epidermal UV-absorbance at a microscopic scale. This study was done on oak (*Quercus petraea*) leaves that were used as a model of woody dicotyledonous leaves.
• *Methods* The leaf development of 2-year-old trees, grown outdoors, was monitored, at a macroscopic scale, by *in vivo* measurements of chlorophyll content per unit area and epidermal UV-absorbance using two optical leaf-clip meters. The distribution of pigments within leaves was assessed *in vivo* spectroscopically. The microscopic images of UV-induced fluorescence and UV-absorbance acquired *in vivo* during leaf development were interpreted from spectral characteristics of leaves.
• *Key Results* At a macroscopic scale, epidermal UV-absorbance was high on the upper leaf side during leaf development, while it increased on the lower leaf side during leaf expansion and reached the adaxial value at maturity. At a microscopic scale, in immature leaves, for both leaf sides, the spatial distribution of epidermal UV-absorbance was heterogeneous, with a pattern depending on the flavonoid content of vacuoles in developing epidermal cells. At maturity, epidermal UV-absorbance was uniform.
• *Conclusions* The spatial pattern of epidermal UV-screen over the area of oak leaves is related to leaf anatomy during development. *In vivo* spectroscopy and fluorescence imaging of the leaf surface showed the distribution of pigments within the leaf and hence can provide a tool to monitor optically the leaf development in nature.

Key words: Blue-green fluorescence, chlorophyll fluorescence, epidermis, flavonoids, leaf development, microscopic imaging, polyphenols, *Quercus petraea*.

INTRODUCTION

In the field, epidermal phenolic compounds constitute a vital screen that protects leaves from damage by natural ultraviolet (UV) radiation (Caldwell *et al.*, 1983). The effectiveness of epidermal UV-screening depends not only on leaf anatomy and content of UV-screening pigments, but also on their uniformity over the leaf area (Day *et al.*, 1993). During leaf development, epidermal thickening and the accumulation of phenolic compounds increase the effectiveness of epidermal UV-screening (DeLucia *et al.*, 1992; Ruhland and Day, 1996). However, the changes in spatial distribution of epidermal UV-screening over the leaf area during leaf development have not been investigated before, although they may have important consequences on the protection of developing leaves against UV light.

To investigate epidermal UV-absorbance in the field, researchers have developed portable leaf-clips, like Dualex and UV-A PAM fluorimeters, which were described earlier (Bilger *et al.*, 2001; Goulas *et al.*, 2004; Pfündel *et al.*, 2007). These fluorimeters measure the UV absorbance of the leaf epidermis by double excitation of chlorophyll *a* fluorescence (ChlF; all abbreviations are defined in Appendix I), according to Bilger *et al.* (1997), using UV (375 nm) and visible (650 nm, in the case of Dualex) light. Epidermal UV-absorbance is determined from the UV/red ChlF excitation ratio (FER). Red light is not absorbed by the epidermis and fully penetrates into the mesophyll where it excits chlorophyll. Therefore, red-excited ChlF can serve as a reference signal to which UV-excited ChlF can be related. Red excitation light is also not absorbed by anthocyanins (Pfündel *et al.*, 2007) that often occur in immature foliage (Hughes *et al.*, 2007). On the other hand, absorbance at 375 nm is mainly due to soluble flavonoids in epidermal vacuoles (Cerovic *et al.*, 2002). Actually, these fluorimeters measure a mean epidermal UV-absorbance over a 5-mm-diameter leaf area and therefore do not spatially resolve the epidermal UV-screening over the leaf area. Thus, multispectral fluorescence imaging has been developed to visualize, non-invasively, the epidermal UV-absorbance over the whole leaf area by using the concept of double excitation of ChlF (Lenk and Buschmann, 2006; Lenk *et al.*, 2007). This macroscopic imaging method has to

* For correspondence. E-mail sylvie.meyer@u-psud.fr

be complemented by microscopic observations to spatially resolve UV-absorbance at the scale of epidermal cells and to investigate the spatial pattern of flavonoid accumulation in epidermal vacuoles in developing leaves.

The interpretation of multispectral fluorescence images of the leaf surface is based on the *in vivo* estimation of the nature and location of fluorophores and UV-absorbing compounds within leaves by using fluorescence emission and excitation spectra (Buschmann and Lichtenthaler, 1998; Cerovic *et al.*, 1999; Cerovic *et al.*, 2002; Lenk and Buschmann, 2006). Under UV-excitation, dicotyledonous green leaves emit blue-green fluorescence (400–630 nm; Cerovic *et al.*, 1999), mainly from hydroxycinnamic acids bound to cell walls and cuticle (Hartley and Harris, 1981; Lang *et al.*, 1991, 1994) and red (630–700 nm) and far-red (700–800 nm) fluorescence from chlorophyll *a* in the mesophyll (for reviews, see Buschmann and Lichtenthaler, 1998; Cerovic *et al.*, 2002). Fluorescence emission spectra have been characterized for mature and senescent dicotyledonous leaves (Lang and Lichtenthaler, 1991; Subhash *et al.*, 1999), and used to interpret the difference of the spatial pattern of fluorescence between adaxial (upper) and abaxial (lower) leaf surfaces (Lang *et al.*, 1994; Lenk and Buschmann, 2006). However, early processes of leaf development have not been studied. They result in chlorophyll synthesis (Niinemets *et al.*, 2004) and flavonoid accumulation at emergence (Salminen *et al.*, 2004), while epidermal and mesophyll cells are dividing and expanding (Avery, 1932). All these changes may strongly affect the spatial pattern of UV-induced fluorescence emission, ChlF excitation and therefore epidermal UV-absorbance on both leaf sides.

In this study, oak was used as a model of woody dicotyledonous species from temperate forest, since their leaves have typical anatomy that is bifacial, heterobaric and hypostomatous (Esau, 1953). The developmental variations in chlorophyll content (Gond *et al.*, 1999) and in leaf phenolic compounds (Covelo and Gaillardo, 2001; Salminen *et al.*, 2004) in field-grown trees are known for this genus. Quercetin derivatives, together with those of kaempferol, represent the dominant flavonoids in oak leaves (Bate-Smith, 1962; Salminen *et al.*, 2004).

Therefore, the aims of this study were (*a*) to characterize the *in vivo* fluorescence emission and UV-absorption of oak leaves and to investigate the spatial pattern of UV-induced visible fluorescence during leaf development, (*b*) to map the epidermal UV-absorbance in immature and mature leaves using the method of the double ChlF excitation at a microscopic scale, and (*c*) to investigate the relationship between anatomical development and optically assessed biochemical development of leaves.

MATERIALS AND METHODS

Plant material and experimental design

Sessile oaks [*Quercus petraea* (Matt.) Liebl.] were grown outdoors in pots in commercial nurseries at Alençon (48°25′50″N, 00°05′35″E). In December 2005, 2-year-old trees about 1·5 m tall were planted in 90-L pots containing a sand/compost mixture (50/50, v/v) without the addition of fertilizer. The pots were spaced 2 m apart in an open field on the campus of the University of Paris-Sud (48°42′N, 02°10′E, France, at an elevation of 65 m). The pots were wrapped in plastic bags to exclude rainfall. The trees were watered once a week (12 L of water per pot, corresponding to the field capacity). One tree among the 70 trees used for other experiments (Maunoury-Danger, 2007), was used for this study. Bud burst took place at day of year (DOY) 105 (mid-April 2007).

Eight DOY were chosen during the growth for sampling, corresponding to key developmental stages, according to Maunoury-Danger (2007). At each sampling date, two leaves per tree were harvested from a south-west-facing branch at around 1100 h and kept in a Petri dish in a humid atmosphere under ambient low light. Chlorophyll and epidermal phenolic compound contents were optically assessed using portable leaf-clip devices, the SPAD chlorophyll meter (hereafter referred to as SPAD) and the Dualex fluorimeter (hereafter referred to as Dualex), respectively, just before recording the excitation and emission spectra. Then, the leaves were stored overnight at low temperature and examined microscopically the following day at an imaging facility (Imaging of Dynamic Processes in Cell and Developmental Biology, Institut Jacques Monod, Paris, France).

Optical measurements of content of chlorophyll and epidermal phenolic compounds in leaves

Chlorophyll content per unit area was estimated with a SPAD-502 chlorophyll meter (Minolta, Carrière-sur-Seine, France). Five measurements were taken on the leaf, at different places, with the SPAD light emitters at the adaxial surface, according to Cartelat *et al.* (2005). Phenolic compounds per unit area were estimated at approximately the same location as the SPAD readings using the Dualex fluorimeter (FORCE-A, Orsay, France). In oak leaves, the Dualex mainly detected flavonols that absorb at 375 nm. Ten Dualex readings (DA_{375}) were taken per leaf, five per leaf side. The DA_{375} values of each side were summed to estimate the total content of phenolic compounds in the leaf epidermis (Cartelat *et al.*, 2005). Relative SPAD and Dualex values were used.

Spectroscopy

ChlF emission and excitation spectra were recorded on a Cary Eclipse spectrofluorimeter (Varian Inc., Les Ulis, France) as described (Bidel *et al.*, 2007). ChlF excitation spectra were scanned from 300 to 700 nm for an emission wavelength of 750 nm, corresponding to the far-red maximum of ChlF emission in intact leaves (Cerovic *et al.*, 1999). Emission spectra were acquired under three excitation wavelengths, UV (365 nm), blue (460 nm) and red (628 nm). All the spectra were from the same median position on the blade between the major veins on both leaf sides. Spectra were measured on 6-mm-diameter areas of the leaf surface at room temperature (around 20°C) under dim light. Leaves were acclimated to these conditions before measurements. Spectra were fully corrected for excitation efficiency and detection response of the spectrofluorimeter and expressed in quinine sulphate-equivalent units (QSEU) to allow a

quantitative comparison among spectra (Cerovic *et al.*, 1999). One QSEU corresponds to the fluorescence of 1 pmol ml^{-1} of quinine sulphate in a 1 cm layer of 0·105 mol l^{-1} perchloric acid in water (1 pmol cm^{-2}), excited at 347·5 nm and emitted at 450 nm under identical measuring conditions. The spectra were smoothed according to Cerovic *et al.* (2002).

The absorbance difference spectra of both leaf sides and between different DOY were obtained from the logarithm of the ratio of the ChlF excitation spectra (logFER) (Cerovic *et al.*, 2002). Smoothed spectra were normalized prior to logFER calculations, so that the integral between 640 and 660 nm equals one, allowing comparison of logFER spectra between samples, but only when UV-induced ChlF was above 25 QSEU (Bidel *et al.*, 2007).

Fluorescence microscopy

Microscopic images were taken from the same leaf area used for fluorescence spectra. Half of the area was mounted with the adaxial side exposed to the excitation light, and half with the abaxial side exposed to the excitation light. Another area of the leaf, from a symmetrical position on the blade with respect to the main vein, was used as an experimental replicate (four replicates per DOY). Samples were mounted in water with Tween 20 (0·5%, v/v) (Sigma, St Louis, USA). Images of fluorescence were made with an inverted epifluorescence microscope (Axiovert 200, Zeiss, Göttingen, Germany) with a monochrome cooled CCD camera (AxioCam MRm, Zeiss, Germany) and a colour cooled CCD camera (AxioCam HRc, Zeiss, Germany). A 100-W mercury vapour lamp (HBO, Zeiss, Germany) provided the excitation light. Leaf fluorescence was imaged using four filter sets described in the Appendix II. Images of 1388 × 1040 pixel size corresponded to an area of 1·7 × 1·3 and 0·22 × 0·17 mm^2 at ×5 and ×40 magnification (Plan-Neofluar quartz objectives, Zeiss), respectively. Monochrome and colour images were stored at 12-bit and 14-bit resolution, respectively. Experiments were automated using Axio Vision software (AxioVision 4·4, Zeiss, Germany) and images were processed using Image J 1·36b (National Institutes of Health, USA).

Imaging of UV-absorbance

Microscopic images were made on a fluorescence standard (0·5 × 0·5 cm^2 piece of plastic filter, Urban blue, Rosco, Sydenham, London, UK) and samples of two types: leaf samples and artificial screens (0·5 × 0·5 cm^2; Lee Filters, Andover, UK) superimposed on a 0·5 × 0·5 cm^2 fluorescence standard. All samples were mounted as described. Twelve Lee filters were selected to cover UV-absorbance from 0·2 to 2·4, corresponding to the Dualex range. With these artificial screens, different methods of UV-absorbance estimation could be compared (Pfündel *et al.*, 2007). In this study, Dualex and microscopic imaging were compared.

Images of epidermal UV-absorbance at 365 nm (MA_{365}) were computed according to the logFER method (Cerovic *et al.*, 2002). At a given magnification, two images of far-red ChlF were successively acquired, one excited by red light using the first filter set ($^{628}MF_{far\text{-}red}$), the other excited by UV light using the second filter set ($^{365}MF_{far\text{-}red}$). These images were from the fluorescence standard and the samples. All images were corrected for optical heterogeneity. A map of MA_{365} was computed pixel by pixel, at 32-bit resolution, by taking into account the differences in time exposure (t) between images of $^{628}MF_{far\text{-}red}$ and $^{365}MF_{far\text{-}red}$ according to:

$$MA_{365} = \log[\text{FER sample}/(\text{FER standard}/10^{0.1})] \quad (1)$$

with

$$\text{FER} = (^{628}MF_{far\text{-}red} \times t_{365})/(^{365}MF_{far\text{-}red} \times t_{628}) \quad (2)$$

To compare MA_{365} with DA_{375} values, the FER of the standard was divided by $10^{0.1}$, where 0·1 was the Dualex measurement on the fluorescence standard (the absorbance difference between 628 and 375 nm). The FER of the artificial screens was corrected for transmission of plastic filters at 628 nm. Frequency distribution histograms were computed from images of MA_{365} with 32-bit resolution.

There was a linear correlation between the mean value of MA_{365} and the DA_{375} values from the 12 Lee filters, with the ×40 objective ($MA_{365} = 0{\cdot}99 \times DA_{375} - 0{\cdot}036$, $r^2 = 0{\cdot}98$, $P < 0{\cdot}0001$, $n = 50$) and the ×5 objective ($MA_{365} = 0{\cdot}46 \times DA_{375} + 0{\cdot}080$, $r^2 = 0{\cdot}97$, $P < 0{\cdot}0001$, $n = 41$). Using the ×5 objective, the mean value of MA_{365} underestimated the DA_{375} value because $^{365}MF_{far\text{-}red}$ is overestimated by scattering light (S). The decreasing exponential relationship between the mean value of $^{365}MF_{far\text{-}red}$ and the DA_{375} values provided an estimate of S (mean $^{365}MF_{far\text{-}red} = 996 + 4522 \times \exp^{-1.79*DA375}$ with $S = 996 \pm 58$, $n = 46$; the corresponding regression between 0 and 1·5 unit of absorbance being $\log(\text{mean } ^{365}MF_{far\text{-}red}) = 3{\cdot}66 - 0{\cdot}41 \times DA_{375}$, $r^2 = 0{\cdot}967$, $P < 0{\cdot}0001$, $n = 42$). Therefore, a mean S value was subtracted from $^{365}MF_{far\text{-}red}$ obtained for both samples and fluorescence standard using the ×5 objective. The S value was 1000 for a 12-bit image.

Fluorescence images were also acquired on transverse leaf sections using the first filter set. Sections were cut manually with a razor blade and observed as previously described.

RESULTS

Developmental patterns of SPAD and Dualex values

Figure 1 shows the variation of SPAD, summed DA_{375} and adaxial and abaxial DA_{375} values during leaf development. Three main periods could be defined: (1) an early spring period (until DOY 155 corresponding to late May), during which leaves contained large concentrations of anthocyanins and expanded rapidly, then thickened and stiffened; SPAD value increased; adaxial and abaxial DA_{375} values decreased slightly and increased markedly, respectively; (2) a late spring period (from DOY 155 to DOY 184, corresponding to June), during which leaves were green and fully expanded; SPAD value was more or less constant and both adaxial and abaxial DA_{375} values were similar and high; (3) a summer period (from DOY 184 to DOY 265, corresponding to July to late September), during which leaves were ageing then senescing; SPAD value decreased; DA_{375} values remained stable.

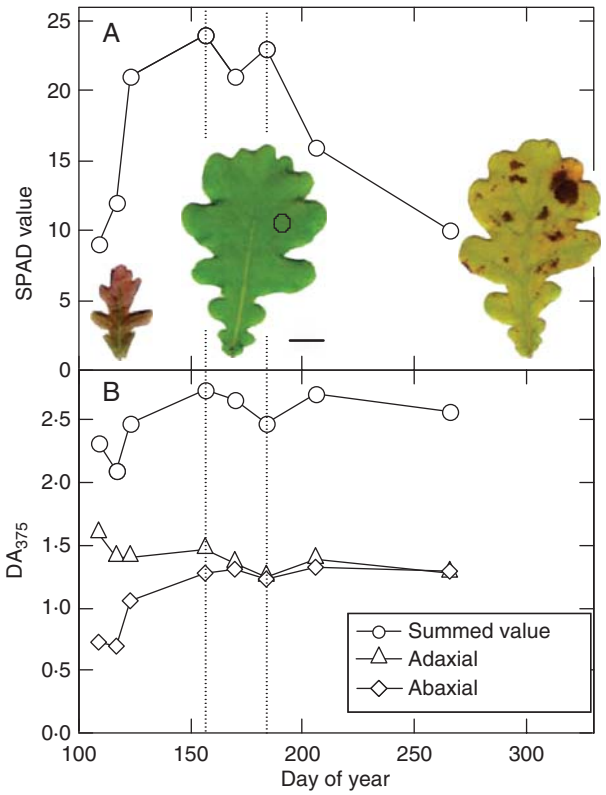

FIG. 1. Developmental variation of SPAD values (A), and DA_{375} summed values and adaxial and abaxial DA_{375} values (B) measured on leaves. Dotted lines at DOY 155 and 183 show the transition from immature to mature leaves and from mature to ageing leaves, respectively. Each point is the mean of two replicates (two leaves). In (A), images are reflectance images of the adaxial side of leaves recorded at DOY 109 (left), 155 (middle) and 265 (right). The scale bar corresponds to 1 cm. The circle on the middle leaf shows the typical site for spectroscopic and imaging measurements.

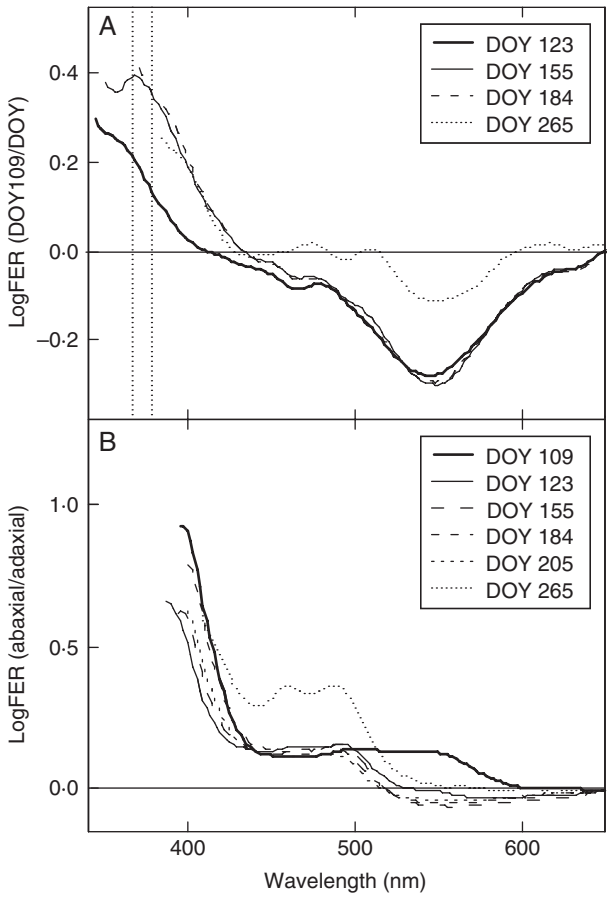

FIG. 2. Absorbance difference spectra obtained from LogFER between each DOY indicated and DOY 109, which was taken as a reference, for the abaxial side (A), and from LogFER between adaxial and abaxial sides of leaves at different DOY (B). The emission wavelength was set at 750 nm for all. In (A), vertical dotted lines are placed at 365 and 375 nm, corresponding to the UV excitation wavelengths used for microscopic and Dualex measurements, respectively. In (B), the spectra at DOY 205 and 184 were similar, therefore, spectra at DOY 184 is the only one shown. In (A) positive values indicate higher absorbance at each DOY indicated compared with DOY 109. In (B) positive values indicate higher absorbance of the adaxial compared with the abaxial leaf side.

Developmental variation of absorbance difference spectra

Absorbance difference spectra of leaves were measured via the logFER parameter, which corresponds to the algebraic difference between spectra. Figure 2A shows the difference between each one of the spectra taken at different DOY to that taken at DOY 109, of the abaxial surface of leaves. Note that UV-induced ChlF from the adaxial leaf side was below the threshold required for accurately calculating the logFER. The logFER value at 365 and 375 nm corresponds to the maximum absorption of band I flavonols (Cerovic *et al.*, 2002; Bidel *et al.*, 2007). As shown in Fig. 1B, logFER values increased from DOY 109 to DOY 155, showing an increase in flavonol content per unit area. Thereafter, logFER values remained stable. LogFER values around 550 nm were negative from DOY 123 onward, indicating an early decrease in anthocyanin content. In the blue-green spectral domain (450–530 nm), the shape of the spectra revealed the presence of carotenoids that increased apparently at DOY 265, due to chlorophyll breakdown during senescence (Fig. 1A).

Figure 2B shows the difference in absorbance, estimated via the logFER parameter, between adaxial and abaxial leaf surfaces throughout leaf development. Note that the logFER spectra could not be calculated for wavelengths below 385–390 nm, because UV-induced ChlF from the adaxial leaf side was below 25 QSEU. Around 390–400 nm, logFER values decreased from DOY 109 to DOY 123, but were stable until DOY 205. At DOY 109, the positive values of logFER around 530 nm suggested higher adaxial anthocyanin content. Thereafter, absorbance at the green waveband was similar on both leaf surfaces. The positive values of logFER around 450–530 nm at each DOY indicated a higher carotenoid content on the adaxial than on the abaxial side.

Developmental variation of fluorescence emission spectra of leaves

To investigate further the nature and the location of leaf fluorophores and absorbing compounds within developing leaves, the fluorescence emission spectra of leaves were recorded using UV, blue and red excitation light.

The absorption profile within leaves of UV, blue and red lights is different, depending on the relative location and content of the main pigments, that is UV-absorbing compounds, carotenoids and chlorophyll (Louis *et al.*, 2006; Buschmann, 2007).

The UV-induced blue-green fluorescence, $^{365}SF_{420-630}$, increased with DOY, in both leaf sides (Fig. 3A, B), therefore it was not affected by the accumulation of UV-absorbing flavonoids in the epidermis. This suggests that $^{365}SF_{420-630}$ originated mostly from the leaf surface. The shape of the emission spectra changed during leaf development. This suggests that the nature of blue-green fluorophores changed and this could reveal that $^{365}SF_{420-630}$ emanated also from the mesophyll where carotenoids and chlorophyll reabsorbed it. On the abaxial side, a background of wide-band fluorescence or

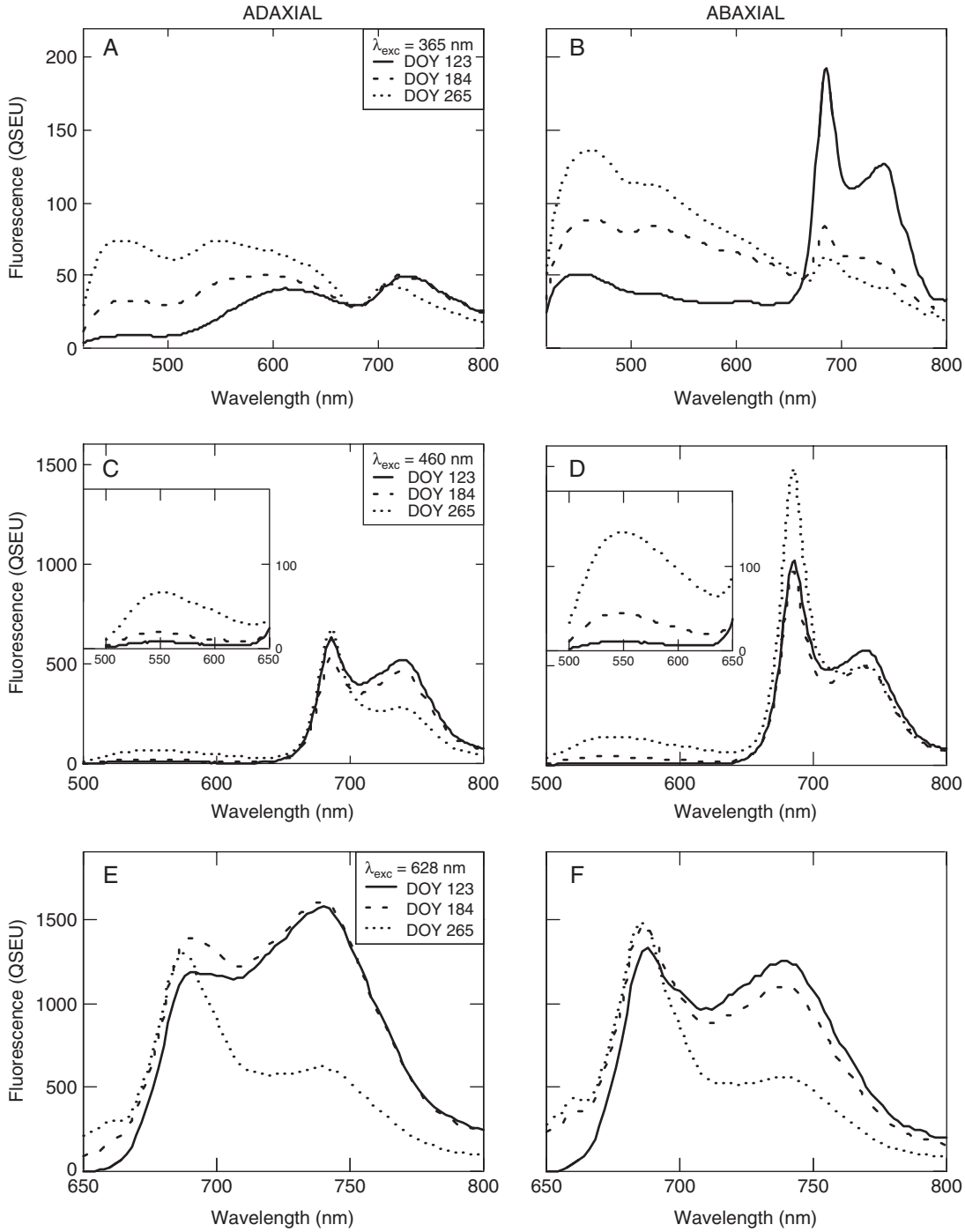

FIG. 3. Fluorescence emission spectra acquired on adaxial (A, C, E) and abaxial (C, D, F) sides of leaves at DOY 123, 184 and 265. The excitation wavelength was set at 365 nm (A, B), 460 nm (C, D) and 628 nm (E, F). In (C) and (D), the inserts show the detail of the emission spectra in the range of green to red fluorescence (500–650 nm). In (E) and (F), fluorescence emission was acquired with a RG665 filter at DOY 123 and a RG645 filter at DOY 184 and 265.

stray light in this spectral domain increased with DOY and might be due to cuticle thickening, or enlargement of intercellular spaces in spongy parenchyma. UV-induced red ($^{365}SF_{680}$) and far-red ($^{365}SF_{740}$) ChlF were low on the adaxial side and decreased with DOY on the abaxial side (Fig. 3A, B), suggesting the accumulation of UV-absorbing compounds, as shown in Figs 1B and 2A. Under blue excitation light, the fluorescence emitted between 500 and 630 nm ($^{470}SF_{530-630}$) was low, but increased with DOY, especially at DOY 265, during chlorophyll breakdown (Fig. 3C, D). Hence, the corresponding fluorophores could be in the mesophyll. The ChlF emission peaks, $^{460}SF_{680}$, $^{460}SF_{740}$, $^{628}SF_{680}$ and $^{628}SF_{740}$, were very close between DOY 123 and 184, suggesting a similar chlorophyll distribution within the mesophyll (Fig. 3C–F). At DOY 265, the $^{460}SF_{740}$ and $^{628}SF_{740}$ decreased, especially on the adaxial side, since the chlorophyll breakdown decreased the ChlF reabsorption. The difference in the shape of the spectra between the adaxial (Fig. 3A, C, E) and the abaxial (Fig. 3B, D, F) surface is clearly related to the dorso-ventral asymmetry characteristic of dicotyledonous leaves (Lang and Lichtenthaler, 1991; Louis *et al.*, 2006; Buschmann, 2007) and especially showed that chlorophyll and carotenoid density was higher in palisade parenchyma than in spongy parenchyma from DOY 123 onwards.

Anatomical origin of UV-induced visible fluorescence throughout development

Images of leaf transverse sections show that blue-green fluorophores were apparent in cell walls, abaxial trichomes and the adaxial cuticle from DOY 123 onwards, once the leaf was fully expanded and began to thicken and stiffen (Fig. 4). The final thickness of the leaf was reached at DOY 184.

Images of UV-induced visible fluorescence over each leaf side show the minor leaf venation delimiting the small areas of mesophyll, termed areoles (Fig. 5). The ChlF emission was patchy in areoles at DOY 123 (Fig. 5A, E) on both leaf sides and at DOY 155 on the abaxial side (Fig. 5F), suggesting heterogeneous accumulation of UV-screening compounds at the surface of immature leaves. From DOY 184 onwards, ChlF emission became more uniformly low (Fig. 5C–H). At DOY 265, some clusters of bright blue fluorescing epidermal cells appeared on the adaxial side (Fig. 5D, insert) and may have contributed towards the increase in $^{365}SF_{420-630}$ (Fig. 3A). On the abaxial side, blue fluorescence emanated from stomata, trichomes and veins (Fig. 5H).

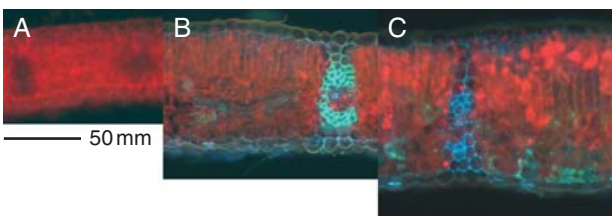

FIG. 4. Colour fluorescence images of leaf transverse sections at DOY 109 (A), 123 (B) and 184 (C). The fluorescence was excited at 365 nm, using the first filter set (cf. Appendix II).

Map of epidermal UV-absorbance in immature and mature leaves

Figures 6 and 7 show images of $^{628}MF_{far\text{-}red}$, $^{365}MF_{far\text{-}red}$, the calculated image of MA_{365} and the corresponding frequency distribution for both sides of immature and mature leaves.

In immature leaves, at DOY 109, MA_{365} of the adaxial side was heterogeneous, with patchy areoles at a distance from the main vein (Fig. 6). Areoles covered 58 % of the imaged leaf area with a mean MA_{365} of $0{\cdot}93 \pm 0{\cdot}08$ (Fig. 6C). MA_{365} was approx. 0·8 in veins. The patchy pattern of MA_{365} images was related to that of $^{365}MF_{far\text{-}red}$ (Fig. 6B). In contrast, the $^{628}MF_{far\text{-}red}$ of areoles was uniform and was the highest along the main vein, where the mesophyll was thickest. The frequency distribution of MA_{365} was uni-modal, with a shoulder for low values of MA_{365} that corresponded to veins and patches in areoles (Fig. 6D). On the abaxial side, the heterogeneous distribution of MA_{365} was related to the leaf venation (Fig. 6G). MA_{365} was lower in areoles than in minor veins and in the perivascular area of the main veins. This pattern was related to that of $^{365}MF_{far\text{-}red}$ (Fig. 6F), whereas $^{628}MF_{far\text{-}red}$ was more uniform (Fig. 6E). Mean MA_{365} in areoles was $0{\cdot}73 \pm 0{\cdot}03$, and areoles covered 52 % of the area imaged. MA_{365} was approx. 0·8 in the veins. The frequency distribution of MA_{365} was large but uni-modal, therefore the difference in MA_{365} between veins and areoles was slight (Fig. 6H).

In mature leaves, at DOY 184, on the adaxial side, images of $^{628}MF_{far\text{-}red}$ and $^{365}MF_{far\text{-}red}$ were almost uniform in areoles (Fig. 7A, B). MA_{365} was uniformly high in areoles and low in veins (Fig. 7C). Mean MA_{365} in areoles was $1{\cdot}1 \pm 0{\cdot}04$. Areoles covered 71 % of the leaf area considered. The frequency distribution of MA_{365} was uni-modal, with a large skew to the left that corresponded to veins (approx. 0·9; Fig. 7D). On the abaxial side, images of $^{628}MF_{far\text{-}red}$, $^{365}MF_{far\text{-}red}$ and MA_{365} showed patches in areoles that corresponded to stomata (Fig. 7E–G). Mean MA_{365} in areoles was $0{\cdot}93 \pm 0{\cdot}05$. Areoles covered 59 % of the surface imaged (Fig. 7G) and corresponded to the left shoulder of the frequency distribution, the main peak of which was due to veins (approx. 1·04; Fig. 7H). Note that, in Fig. 7, the MA_{365} was not the true one for epidermal cells situated above the veins because, in these areas, the cells below the epidermis did not contain chlorophyll (see Fig. 4C). The slight ChlF detected in vein areas (Fig. 7A, B, E and F) could be a diffuse one emanating from the surrounding mesophyll. Hence, the relatively high MA_{365} in veins compared with areoles (Fig. 7G) that contrasted with the pattern observed on the adaxial side (Fig. 7C) suggests that the adaxial $^{365}MF_{far\text{-}red}$ in vein areas was enhanced by diffuse ChlF emanating from the palisade parenchyma.

The heterogeneous spatial pattern of MA_{365} at DOY 109 (Fig. 6) was related to the UV-absorbance of individual epidermal cells, for both leaf sides (Figs 8 and 9). On the adaxial side, at DOY 109, the value of MA_{365} was around 1·2 and 1·3 in low and high UV-screening cells, respectively (Fig. 8A, insert). At DOY 123, the patchiness continued to characterize epidermal cells, enlarged by 2-fold as the leaf grew (Fig. 8B). At DOY 184, MA_{365} was uniformly distributed over all epidermal cells, with a high mean value of $1{\cdot}4 \pm 0{\cdot}02$ (Fig. 8C), the maximum values being in vacuoles. On the

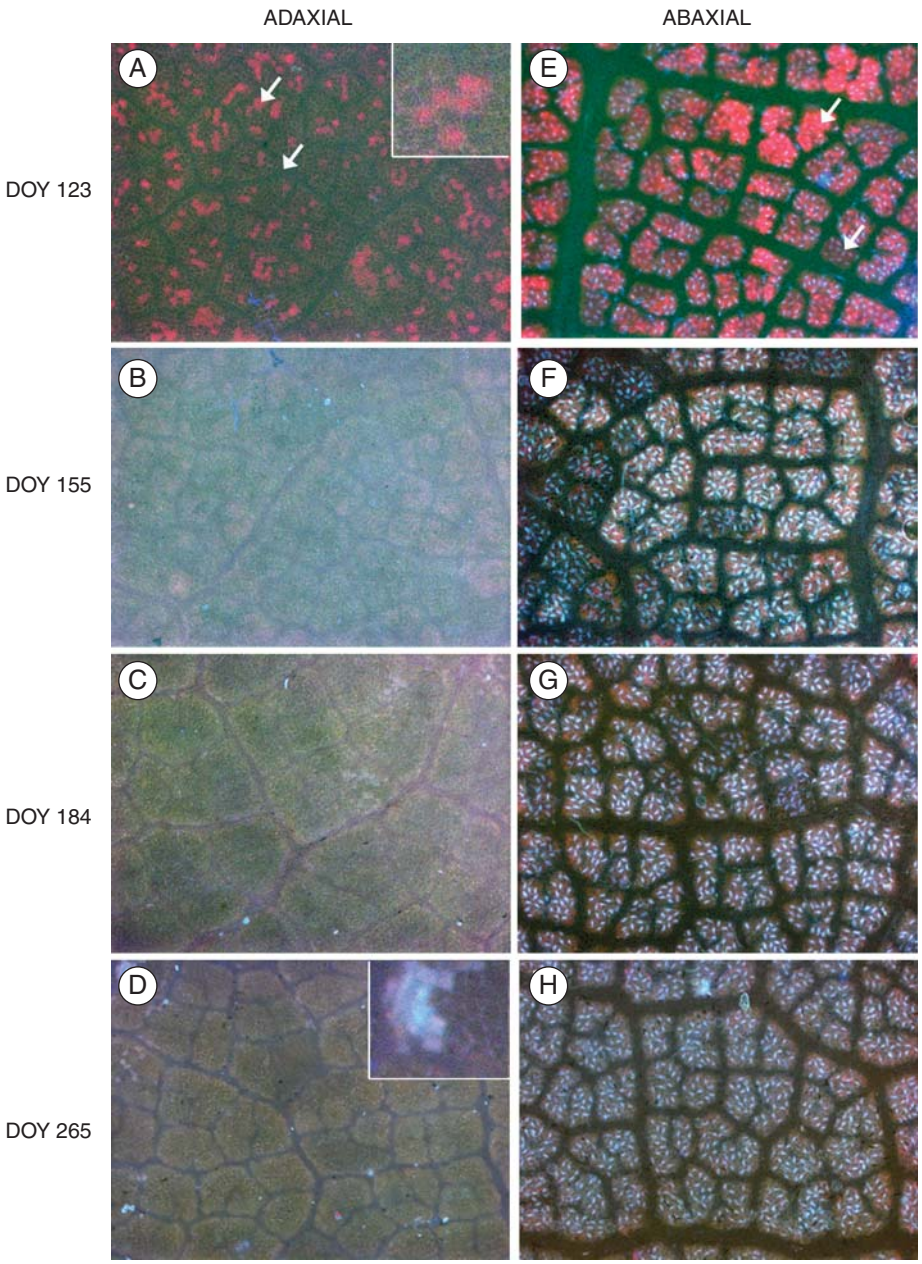

FIG. 5. Colour fluorescence images of adaxial (A–D) and abaxial (E–H) sides of leaves at DOY 123 (A, E), 155 (B, F), 184 (C, G) and 265 (D, H). The fluorescence was excited at 365 nm, using the first filter set (cf. Appendix II). Images were taken with ×5 magnification and correspond to 2·2 mm^2 leaf area. On the abaxial side, bright blue spots are stomata. In (A) and (D), inserts are details zoomed in by 3 times. In (A) and (D), upper and lower arrows show areas where relative ChlF is high and low, respectively.

abaxial side at DOY 109 (Fig. 9A), mean MA_{365} was 1·1 ± 0·02 and 0·96 ± 0·02 in veins and areoles, respectively. The value of MA_{365} varied according to the cell vacuolation. Small and undifferentiated epidermal cells, that seemed to result from a recent mitosis, contained several small vacuoles exhibiting a relatively low value of MA_{365} (Fig. 9D, upper arrow). They juxtaposed large epidermal cells containing a large vacuole exhibiting a relatively high MA_{365} value (Fig. 9D, lower arrow). A high value of MA_{365} was also observed in the vacuole of differentiating stomata (Fig. 9E, upper arrow). At DOY 123 and 184 (Fig. 9B, C and F), areoles were enlarged but the corresponding MA_{365} remained lower than in veins. In differentiated stomata, chloroplasts appeared as dark spots showing no UV-screening of the excitation light responsible for stomatal ChlF emission (Fig. 9F).

DISCUSSION

The results show heterogeneous epidermal UV-absorbance in immature leaves (DOY 109 and 123). This was not due to a heterogeneous distribution of chlorophyll since images of $^{628}MF_{far\text{-}red}$ and images of reflectance (not shown) were

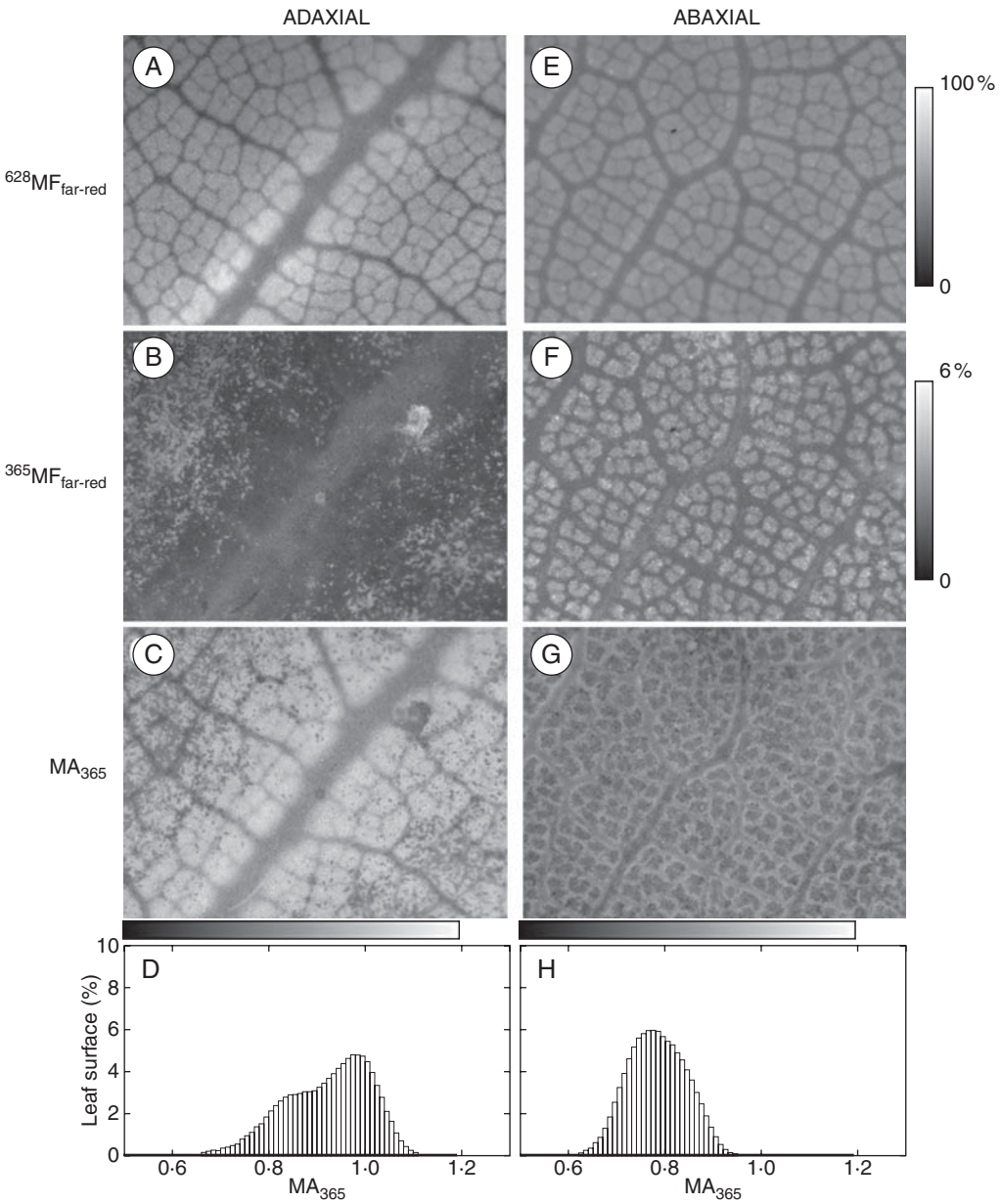

FIG. 6. Fluorescence images ($^{628}MF_{far-red}$ and $^{365}MF_{far-red}$), UV absorbance images (MA_{365}) and frequency distributions of MA_{365} of a leaf at DOY 109. Adaxial (A–D) and abaxial (E–H) sides of the leaf were imaged with a ×5 objective. $^{365}MF_{far-red}$ was corrected for the light background *S*. Images correspond to 2·2 mm^2 leaf area. Pixel intensity was scaled using an 8-bit grey scale, where black and white corresponded to a relative fluorescence intensity of 0 and 100 % (A, E), or 0 and 6 %, respectively (B, F). In (C) and (G), black and white pixels correspond to 0·5 and 1·2, respectively, and the grey scale corresponds to the numerical scale of the top *x*-axis of (D) and (H), from 0·5 to 1·2. Mean MA_{365} and s.d. are 0·92 ± 0·09 (D) and 0·78 ± 0·06 (H). The class size is 0·01 (E, H).

uniform in areoles. Therefore lower $^{365}MF_{far-red}$ in areoles was associated with higher epidermal UV-absorbance. Furthermore, the MA_{365} heterogeneity was not induced by Tween 20, which is non-ionic and non-toxic. Moreover, the refractive index of Tween 20 is 1·47, which is close to that of cell walls (1·42; Vogelmann *et al.*, 1996).

MA_{365} values were not strictly similar to DA_{375} values, despite corrections by *S*, inter-calibration and the measurement of far-red ChlF that was not reabsorbed (Buschmann, 2007). However, DA_{375} and MA_{365} were not obtained by using exactly the same excitation wavelengths and the DA_{375} value was a mean over a larger area than the mean MA_{365} (see Appendix I); therefore, depending on the pattern of heterogeneity, DA_{375} and mean MA_{365} values could be different. Actually, the complexity of the leaf optical properties (cf. Kim *et al.*, 2001) and the inherent limits of the logFER method (Agati *et al.*, 2005; Kolb and Pfündel, 2005; Lenk *et al.*, 2007) still restricted the fully quantitative correspondence between macroscopic and microscopic measurements of UV-absorbance over the leaf area. Nevertheless, there was a general accordance between the developmental pattern of DA_{375} (Fig. 1B), spectroscopy (Figs 2 and 3A and B), fluorescence imaging (Fig. 5) and UV-absorbance mapping (Figs 6–9). The spatial pattern of UV-induced fluorescence

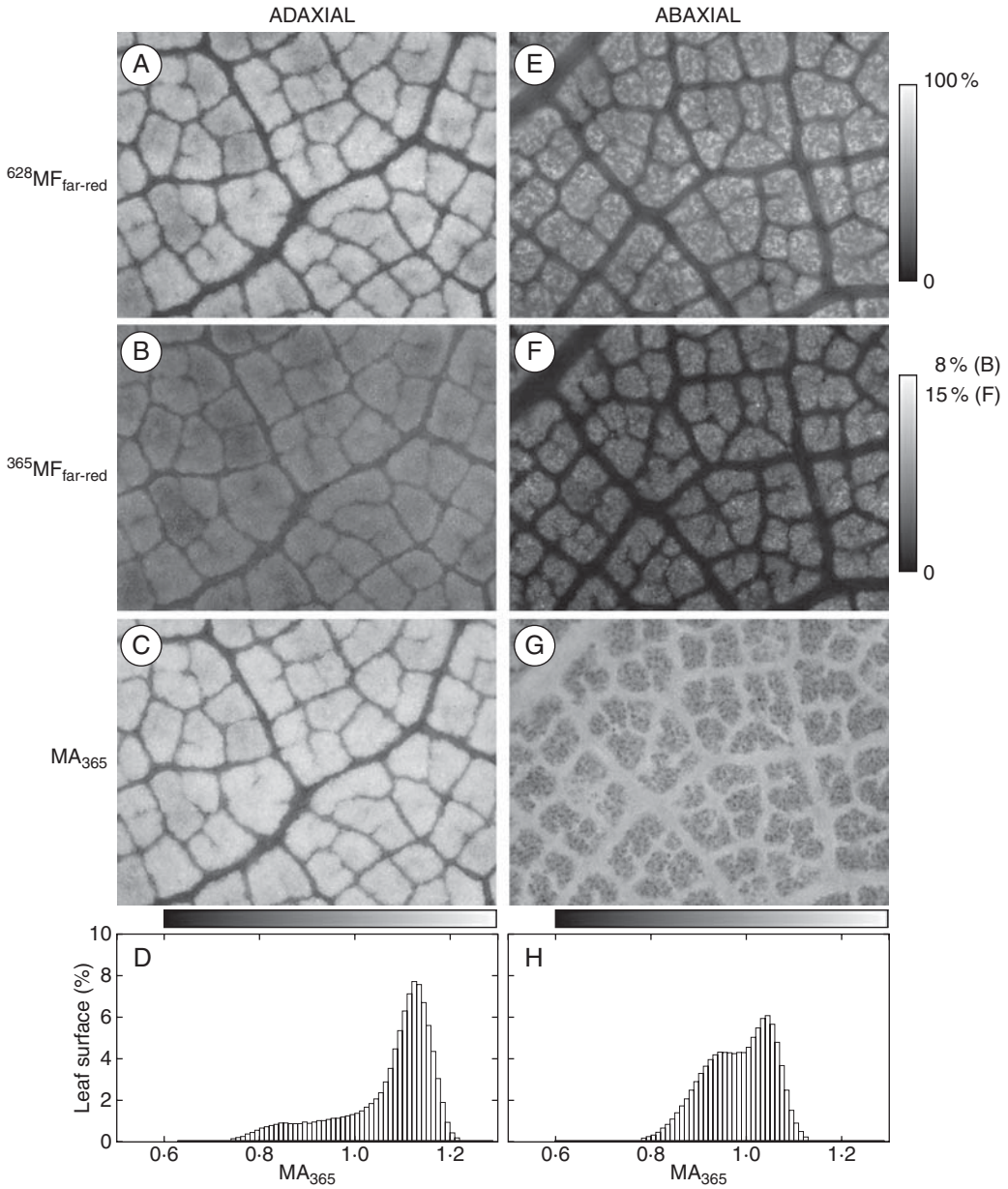

FIG. 7. Fluorescence images ($^{628}MF_{far\text{-}red}$ and $^{365}MF_{far\text{-}red}$), UV absorbance images (MA_{365}) and frequency distributions of MA_{365} of a leaf at DOY 184. Adaxial (A–D) and abaxial (E–H) sides of the same leaf were imaged with a ×5 objective. $^{365}MF_{far\text{-}red}$ was corrected for the light background *S*. Images correspond to 2·2 mm^2 leaf area. Pixel intensity was scaled using an 8-bit grey scale where black and white correspond to a relative fluorescence intensity of 0 and 100 % (A, E), 0 and 8 % (B) or 0 and 15 % (F), respectively. In (C) and (G), black and white pixels correspond to 0·6 and 1·3, respectively, and the grey scale corresponds to the numerical scale of the top *x*-axis of (D) and (H), from 0·6 to 1·3. Mean MA_{365} and s.d. are 1·1 ± 0·10 (D) and 0·98 ± 0·07 (H). The class size is 0·01 (E, H). In (F) and (G), bright and dark patches in areoles corresponded to stomata, respectively.

images (Fig. 5) was in accordance with the MA_{365} pattern acquired at ×5 (with *S* correction, Figs 6 and 7) and ×40 (no *S* correction, Figs 8 and 9) magnifications. Therefore, images of MA_{365} accurately depicted the spatial pattern of epidermal absorbance at 365 nm.

In immature leaves (until DOY 155), anthocyanins decreased as leaves expanded, as previously reported (Coley and Barone, 1996; Hughes *et al.*, 2007); the abaxial flavonoid content per unit area increased, indicating a gradual acclimation of leaves to natural UV light. Adaxial and abaxial epidermises were not uniform UV-screens for the developing mesophyll. The accumulation of flavonoids in the vacuole varied from cell to cell and reflected the asynchronous development of epidermal cells (Avery, 1932). The spatial pattern of MA_{365} on the abaxial side suggested that epidermal cells situated above veins accumulated the first flavonoids. Immature leaves are sinks, importing sugar through phloem from tree storage to synthesize soluble phenolic compounds (Kleiner *et al.*, 1999). Therefore, the spatial distribution of MA_{365} might reflect micro sink–source relationships. The epidermal cells close to the importing area might accumulate flavonoids in vacuoles earlier than distant epidermal cells. A strong

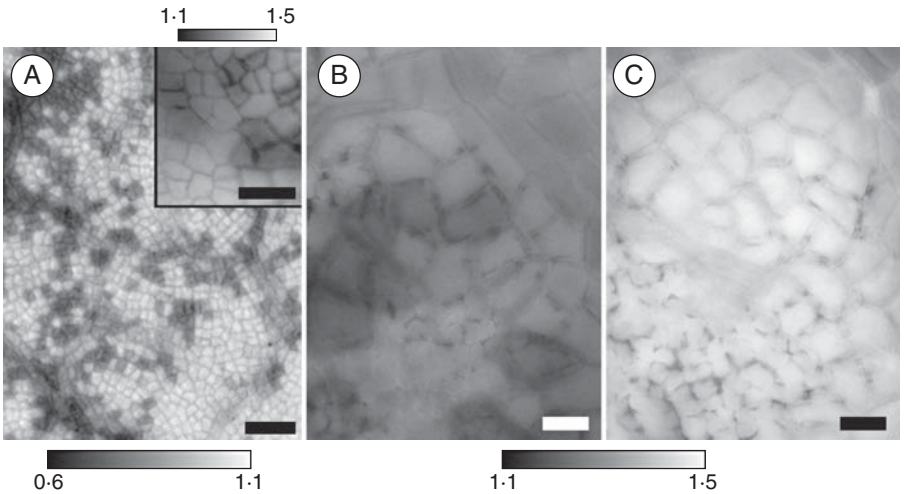

FIG. 8. Images of MA_{365} of the leaf adaxial side at DOY 109 (A), 123 (B) and 184 (C). Black and white pixels correspond to 0·6 and 1·1 (A) or 1·1 and 1·5 (insert of A, and B, C), respectively. Images were taken with ×5 (A) and ×40 (insert in A, and B, C) objectives and rescaled in such a way that scale bars correspond to 50 μm (A) and 25 μm (insert in A, and B, C). In (B) and (C), the upper surface of the mesophyll is visible.

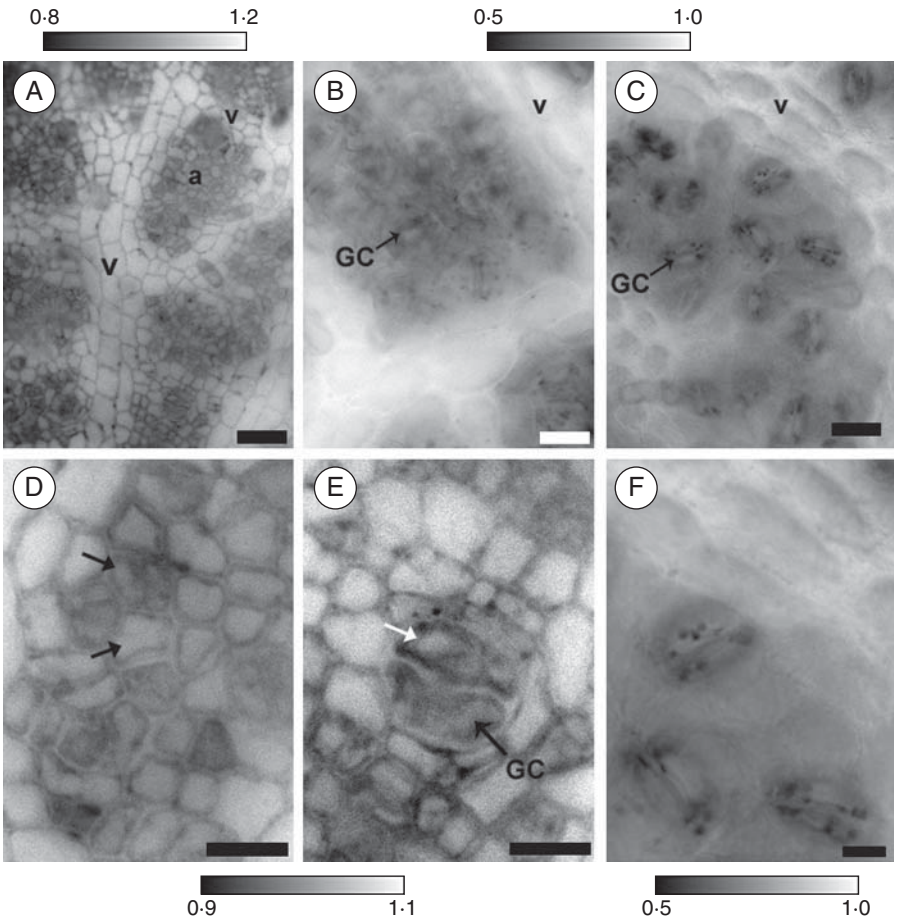

FIG. 9. Images of MA_{365} of the leaf abaxial side at DOY 109 (A, D, E), 123 (B) and 184 (C, F). Black and white pixels correspond to 0·8 and 1·2 (A), 0·5 and 1·0 (B, C, F) or 0·9 and 1·1 (D, E), respectively. Images were taken with a ×40 objective and rescaled in such a way that scale bars correspond to 25 μm (A–C) and 10 μm (D–F). a, Areole; GC, guard cell; v, vein. In (D) the upper and lower arrows show early and late stages of epidermal cell vacuolation, respectively. In (E) the upper arrow shows a vacuole.

dorso-ventral asymmetry in pigment distribution appeared early within developing leaves (DOY 109) since photoprotective pigments (epidermal flavonoids, anthocyanins and carotenoids) were mainly accumulated on the adaxial side, i.e. the one mostly exposed to visible and UV light. Blue-green fluorophores were not apparent at DOY 109 (see Fig. 6) and were accumulated from DOY 123 onwards, mainly on abaxial sides, which bore photoprotective trichomes (Karabourniotis *et al.*, 1995).

In mature leaves (from DOY 155 to DOY 184), adaxial and abaxial epidermal UV-absorbance were similar, high and uniform among areoles (except for stomata). Therefore, both epidermises constituted a uniform UV-screen for the mesophyll, and leaves were uniformly acclimated to natural UV. The increase of $^{365}SF_{420-630}$ from DOY 123 onwards, suggested an accumulation of hydroxycinnamic acids bound to cuticle and cell walls and the lignification of the xylem in veins and bundle sheath extensions (Wiermann, 1981). This could provide not only an additional UV-screen at the leaf surface (Day *et al.*, 1993), but also structural support to the leaf lamina and protection against biotic attacks (Coley and Barone, 1996). Therefore, the $^{365}SF_{420-630}$ could reflect the toughing of leaves. The dorso-ventral asymmetry of $^{365}SF_{420-630}$ was also shown in beech leaves (Lang and Lichtenthaler, 1991) and could result from higher amount of hydroxycinnamic acids on the abaxial side (Bidel *et al.*, 2007) as well as a lower reabsorption of blue fluorescence by abaxial mesophyll (Lang and Lichtenthaler, 1991).

In ageing and subsequent senescing leaves (from DOY 184 to DOY 265), adaxial and abaxial epidermal UV-absorbance remained high and uniform (see Fig. 5). Therefore the mesophyll was protected against UV light during chlorophyll breakdown. The increase in $^{365}SF_{420-630}$ at DOY 265 might result from the decrease in reabsorption by carotenoids and chlorophylls (Lichtenthaler, 1987; Lang and Lichtenthaler, 1991) and the synthesis of blue-green fluorescent phytoalexins (Cerovic *et al.*, 1999) in response to the colonization of the leaf surface by microorganisms, which might be facilitated by a loss of cuticle hydrophobicity (Bringe *et al.*, 2006). The increase of $^{470}SF_{530-630}$ at DOY 265 might be related to local cell necrosis (Bussotti *et al.*, 2005).

In conclusion, spectroscopy and fluorescence imaging allowed an *in vivo* assessment of changes in oak leaf structure and pigments throughout development. $^{365}SF_{450}$ and $^{365}SF_{far\text{-}red}$ excitation increased and decreased with leaf age, respectively, in sessile oak, in beech (Lang and Lichtenthaler, 1991), tobacco (Subhash *et al.*, 1999) and wheat (Meyer *et al.*, 2003), species that exhibit different phytochemistry, anatomy and growth patterns. Therefore, these parameters can provide a signature for *in vivo* phenology monitoring. Microscopic imaging of epidermal UV-absorbance complements the macroscopic imaging (Lenk and Buschmann, 2006) and is a promising tool for investigating further the genetic and environmental controls of flavonoids accumulation and compartmentation in epidermal cells. This is a prerequisite for an effective use of epidermal UV-absorbance and fluorescence parameters in the field to monitor non-invasively the physiological stage of the plant using portable multispectral fluorimeters (Cerovic *et al.*, 2008).

ACKNOWLEDGEMENTS

This work was supported by the French National Centre for Scientific Research (CNRS). We thank Gwendal Latouche (ESE, UMR 8079, CNRS, France) for assistance in choosing the filter set and for helpful discussion, Christophe Chamot (Plate-forme de Recherche 'Imagerie des processus dynamiques en biologie cellulaire et biologie du développement', Institut Jacques Monod, INSERM, CNRS, France) for technical assistance. We are grateful to Jean-Marc Ducruet (ESE, UMR 8079, CNRS, France) and Marine Le Moigne (FORCE-A, France) for helpful comments on the manuscript. American Journal Experts (Durham, USA) reviewed the paper for English usage.

We dedicate this study to the memory of the late Nicolae Moise, an exceptional and friendly researcher without whom this study, like many others, would not have been possible.

LITERATURE CITED

Agati G, Pinelli P, Ebner SC, Romani A, Cartelat A, Cerovic ZG. 2005. Non destructive evaluation of anthocyanins in olive (*Olea euopaea*) fruits by *in situ* chlorophyll fluorescence spectroscopy. *Journal of Agricultural Food Chemistry* **53**: 1354–1363.

Avery GS. 1932. Structure and development of the tobacco leaf. *American Journal of Botany* **20**: 565–592.

Bate-Smith EC. 1962. The phenolic constituents of plants and their taxonomic significance. *Journal Linnean Society –Botany* **58**: 95–175.

Bidel LPR, Meyer S, Goulas Y, Cadot Y, Cerovic ZG. 2007. Responses of epidermal phenolic compounds to light acclimation: *in vivo* qualitative and quantitative assessment using chlorophyll fluorescence excitation spectra in leaves of three woody species. *Journal of Photochemical and Photobiology B. Biology* **88**: 163–179.

Bilger W, Veit M, Schreiber L, Schreiber U. 1997. Measurement of leaf epidermal transmittance of UV radiation by chlorophyll fluorescence. *Physiologia Plantarum* **101**: 754–763.

Bilger W, Johnsen T, Schreiber U. 2001. UV-excited chlorophyll fluorescence as a tool for the assessment of UV-protection by the epidermis of plants. *Journal of Experimental Botany* **52**: 2007–2014.

Bringe K, Schumader CFA, Schmitz-Eiberger M, Steiner U, Oerke E-C. 2006. Ontogenetic variation in chemical and physical characteristics of adaxial apple leaf surfaces. *Phytochemistry* **67**: 161–170.

Buschmann C. 2007. Variability and application of the chlorophyll fluorescence emission ratio red/far-red of leaves. *Photosynthesis Research* **92**: 261–271.

Buschmann C, Lichtenthaler HK. 1998. Principles and characteristics of multi-colour fluorescence imaging of plants. *Journal of Plant Physiology* **152**: 297–314.

Bussotti F, Agati G, Desotgiu R, Matteini P, Tani C. 2005. Ozone foliar symptoms in woody plants assessed with ultrastructural and fluorescence analysis. *New Phytologist* **166**: 941–955.

Caldwell MM, Robberecht R, Flint SD. 1983. Internal filters: prospects for UV-acclimation in higher plants. *Physiologia Plantarum* **58**: 445–450.

Cartelat A, Cerovic ZG, Goulas Y, *et al*. 2005. Optically assessed contents of leaf polyphenolics and chlorophyll as indicators of nitrogen deficiency in wheat (*Triticum aestivum* L.). *Field Crops Research* **91**: 35–49.

Cerovic ZG, Samson G, Morales F, Tremblay N, Moya I. 1999. Ultraviolet-induced fluorescence for plant monitoring: present state and prospects. *Agronomie: Agriculture and Environment* **19**: 543–578.

Cerovic ZG, Ounis A, Cartelat A, *et al*. 2002. The use of chlorophyll fluorescence excitation spectra for the non-destructive *in situ* assessment of UV-absorbing compounds in leaves. *Plant, Cell & Environment* **25**: 1663–1676.

Cerovic ZG, Moise N, Agati G, Latouche G, Ben Ghozlen N, Meyer S. 2008. New portable optical sensors for the assessment of winegrape phenolic maturity based on berry fluorescence. *Journal of Food Composition and Analysis* **21**: 650–654.

Coley PD, Barone JA. 1996. Herbivory and plant defenses in tropical forests. *Annual Review of Ecology and Systematics* **27**: 305–335.

Covelo F, Gaillardo A. 2001. Temporal variation in total leaf phenolics concentration of *Quercus robur* in forested and harvested stands in northwestern Spain. *Canadian Journal of Botany* **79**: 1262–1269.

Day TA, Martin G, Vogelmann TC. 1993. Penetration of UV-B radiation in foliage – evidence that the epidermis behaves as a non-uniform filter. *Plant, Cell & Environment* **16**: 735–741.

DeLucia EH, Day TA, Vogelmann TC. 1992. Ultraviolet-B and visible light penetration into needles of two species of subalpine conifers during foliar development. *Plant, Cell & Environment* **15**: 921–929.

Esau K. 1953. *Plant anatomy*. New York, NY: Wiley and Sons.

Gond V, de Pury DGG, Veroustraete F, Ceulemans R. 1999. Seasonal variations in leaf area index, leaf chlorophyll, and water content; scaling-up to estimate fAPAR and carbon balance in a multilayer, multispecies temperate forest. *Tree Physiology* **19**: 673–679.

Goulas Y, Cerovic ZG, Cartelat A, Moya I. 2004. Dualex: a new instrument for field measurements of epidermal ultraviolet absorbance by chlorophyll fluorescence. *Applied Optics* **43**: 4488–4496.

Hartley RD, Harris PJ. 1981. Phenolic constituents of the cell walls of dicotyledons. *Biochemical Systematics and Ecology* **9**: 189–203.

Hughes NM, Morley CB, Smith WK. 2007. Coordination of anthocyanin decline and photosynthetic maturation in juvenile leaves of three deciduous tree species. *New Phytologist* **175**: 675–685.

Karabourniotis G, Kotsabassidis D, Manetas Y. 1995. Trichome density and its protective potential against ultraviolet-B radiation damage during leaf development. *Canadian Journal of Botany* **73**: 376–383.

Kim MS, McMurtrey JE, Mulvh CL, Daughtry CST, Chappelle EW, Chen YR. 2001. Steady-state multispectral fluorescence imaging system for plant leaves. *Applied Optics* **40**: 157–166.

Kleiner KW, Rafa KF, Dickson RE. 1999. Partitioning of ^{14}C-labeled photosynthate to allelochemicals and primary metabolites in source and sink leaves of aspen: evidence for secondary metabolic turnover. *Oecologia* **119**: 408–418.

Kolb CA, Pfündel EE. 2005. Origins of non-linear and dissimilar relationships between epidermal UV absorbance and UV absorbance of extracted phenolics in leaves of grapevine and barley. *Plant, Cell & Environment* **25**: 580–590.

Lang M, Lichtenthaler HK. 1991. Changes in the blue-green and red fluorescence-emission spectra of beech leaves during the autumnal chlorophyll breakdown. *Journal of Plant Physiology* **138**: 550–553.

Lang M, Stober F, Lichtenthaler H. 1991. Fluorescence emission spectra of leaves and plant constituents. *Radiation and Environmental Biophysics* **30**: 333–347.

Lang M, Lichtenthaler HK, Sowinska M, Summ P, Hiesel F. 1994. Blue, green and red fluorescence signatures and images of tobacco leaves. *Botanica Acta* **107**: 230–236.

Lenk S, Buschmann C. 2006. Distribution of UV-shielding of the epidermis of sun and shade leaves of the beech (*Fagus sylvatica* L.) as monitored by multi-colour fluorescence imaging. *Journal of Plant Physiology* **163**: 1273–1283.

Lenk S, Buschmann C, Pfündel EE. 2007. *In vivo* assessing flavonols in white grape berries (*Vitis vinifera* L. cv. Pinot Blanc) of different degrees of ripeness using chlorophyll fluorescence imaging. *Functional Plant Biology* **34**: 1092–1104.

Lichtenthaler H. 1987. Chlorophyll fluorescence signatures of leaves during the autumnal chlorophyll breakdown. *Journal of Plant Physiology* **131**: 101–110.

Louis J, Cerovic ZG, Moya I. 2006. Quantitative study of fluorescence excitation and emission spectra of bean leaves. *Journal of Photochemistry and Photobiology B: Biology* **85**: 65–71.

Maunoury-Danger F. 2007. *Etude de la signature isotopique du carbone ($\delta^{13}C$) du CO_2 respiré et du cerne en relation avec le fonctionnement de l'arbre*. Thèse de doctorat, Univ Paris-Sud.

Meyer S, Cartelat A, Moya I, Cerovic ZG. 2003. UV-induced blue-green and far-red fluorescence along wheat leaves: a potential signature of leaf ageing. *Journal of Experimental Botany* **54**: 757–769.

Niinemets U, Kull O, Tenhunen JD. 2004. Within-canopy variation in the rate of development of photosynthetic capacity is proportional to integrated quantum flux density in temperate deciduous trees. *Plant, Cell & Environment* **27**: 293–313.

Pfündel EE, Ben Ghozlen N, Meyer S, Cerovic ZG. 2007. Investigating UV screening in leaves by two different types of portable UV fluorimeters reveals *in vivo* screening by anthocyanins and carotenoids. *Photosynthesis Research* **93**: 205–221.

Ruhland CT, Day TA. 1996. Changes in UV-B radiation screening effectiveness with leaf age in *Rhododendron maximum. Plant, Cell & Environment* **19**: 740–746.

Salminen JP, Roslin T, Karonen M, Sinkkonen J, Pihlaja K, Pulkkinen P. 2004. Seasonal variation in the content of hydrolyzable tannins, flavonoid glycosides, and proanthocyanidins in oak leaves. *Journal of Chemical Ecology* **30**: 1693–1711.

Subhash N, Wenzel O, Lichtenthaler H. 1999. Changes in blue-green and chlorophyll fluorescence emission and fluorescence ratios during senescence of tobacco plants. *Remote Sensing and Environment* **69**: 215–223.

Vogelmann TC, Bornman JF, Yates DJ. 1996. Focusing of light by epidermal cells. *Physiologia Plantarum* **98**: 43–56.

Wiermann R. 1981. Secondary plant products and cell and tissue differentiation. In: Stumpf PK, Conn EE. eds. *The biochemistry of plants*. London: Academic Press, 85–116.

APPENDIX I

Abbreviations and usefulness of the parameters acquired using the different optical methods

Abbreviation	Definition	Usefulness for the experiment
ChlF	Chlorophyll fluorescence	ChlF excitation is used to compute the logFER
logFER	Logarithm of the fluorescence excitation ratio (Cerovic *et al.*, 2002)	Parameter providing the absorbance difference spectra between leaf ages or leaf sides Basic parameter used to measure the epidermal UV-absorbance from double excitation of ChlF by UV and red light using the Dualex fluorimeter or microscopic imaging device
DA_{375}	Epidermal UV-absorbance at 375 nm measured with Dualex fluorimeter on intact leaves (Goulas *et al.*, 2004)	*In vivo* macroscopic estimation of the mean epidermal UV-absorbance over a 5-mm-diameter leaf surface (20 mm^2)
MA_{365}	Microscopic image of epidermal UV-absorbance at 365 nm	*In vivo* visualization of the spatial pattern of epidermal UV-absorbance over a 2·2 mm^2 leaf area ($\times 5$ magnification)
$^{\lambda exc}MF_{\lambda em}$	Microscopic image of fluorescence intensity, excited at wavelength λ_{exc} and emitted at wavelength λ_{em}	Basic parameters used to compute MA_{365} using the logFER method
$^{\lambda exc}SF_{\lambda em}$	Fluorescence intensity, excited at wavelength λ_{exc} and emitted at wavelength λ_{em}, determined from fluorescence emission spectra	Spectroscopic parameters acquired *in vivo* on a 6-mm-diameter leaf surface and used to assess the leaf fluorescence properties during development and to interpret fluorescence images

APPENDIX II

Description of the four filter sets used for microscopic fluorescence imaging

No. of the filters set	Excitation filters	Dichroic beamsplitters	Emission filters
Set 1	628/40 (Semrock, Rochester, USA)	650DRLP02 (Semrock)	Long pass RG695 (2·5 mm thick, Schott, Vanves, France)
Set 2	365HT25 (Semrock)	390DRLP02 (Omega, Brattleboro, USA)	Long pass RG695 (2·5 mm thick, Schott)
Set 3	330WB80 (Semrock)	DCLP400 (Omega)	Long pass LP400 (Omega)
Set 4	330WB80 (Semrock)	390DRLP02 (Omega)	450WB80 (Omega)